International Journal of Heat and Mass Transfer 52 (2009) 620–628

Contents lists available at ScienceDirect

International Journal of Heat and Mass Transfer

journal homepage: www.elsevier.com/locate/ijhmt

Transition to a periodic flow induced by a thin fin on the sidewall of a differentially heated cavity

Feng Xu *, John C. Patterson, Chengwang Lei

School of Engineering, James Cook University, Townsville, QLD 4811, Australia

ARTICLE INFO

Article history:
Received 22 March 2008
Received in revised form 14 June 2008
Available online 25 August 2008

Keywords:
Fin
Differentially heated cavity
Oscillations
Heat transfer

ABSTRACT

The transition to a periodic flow induced by a thin fin on the sidewall of a differentially heated cavity is numerically investigated. The numerical results are compared with a previously reported experiment. It is demonstrated that the transient flow obtained numerically shows features consistent with the experimental flow. Based on the present numerical results, the temporal development and spatial structures of the thermal flow around the fin are described, and the separation of the thermal flow above the fin is discussed. It is found that the presence of the fin changes the flow regime and results in the transition of the thermal flow to a periodic flow. The present numerical results also indicate that the unstable temperature configuration above the fin results in intermittent plumes at the leeward side of the fin, which in turn induce strong oscillations of the downstream boundary layer flow. It is demonstrated that the oscillations of the boundary layer flow significantly enhance the heat transfer through the finned sidewall (by up to 23%).

1. Introduction

Natural convection in a differentially heated cavity is one of the classical problems of fluid mechanics and heat transfer, and has wide industrial application. Consequently it has been extensively studied over the past decades. One of the earliest studies of this problem was reported by Bachelor [1], who demonstrated that for sufficiently small Rayleigh numbers, the mode of heat transfer is primarily dominated by conduction. Subsequent investigations (e.g. [2,3]) have focused on steady natural convection flows in the differentially heated cavity.

However, natural convection in industrial systems is usually unsteady. Accordingly, the transition of the natural convection flow in the cavity following sudden heating has been given considerable attention over the last two decades. Based on a scaling analysis, Patterson and Imberger [4] pointed out that the base flow during the transition mainly involves a vertical boundary layer flow, a horizontal intrusion and the flow in the core. In the case of low Rayleigh numbers (smaller than a critical value), the transition is characterized by the following processes: (a) the transition of the vertical boundary layer from unsteady one-dimensional to steady two-dimensional, which is marked by an overshoot of the temperature signal and subsequent travelling waves induced by the leading edge effect (LEE) [5–7]; (b) the formation of horizontal intrusions due to the presence of the horizontal walls; (c) the arrival of the horizontal intrusion from the opposite sidewall which triggers the second group of travelling waves in the vertical boundary layer [8,9]; and (d) the approach to a steady state and the stratification of the core flow [8,10]. In the case with Rayleigh numbers larger than the critical value, it has been reported that the natural convection flow in the cavity approaches a periodic flow [11–13]. If the Rayleigh number is sufficiently large, the natural convection flow in the cavity even becomes fully turbulent, as reported in [14,15].

The flow in different flow regimes determines heat transfer through the cavity, and thus it is possible to either enhance or depress heat transfer by manipulating the transition of the flow. One of the simplest techniques for enhancing or depressing heat transfer through a differentially heated cavity is to place a horizontal fin on the heated or cooled sidewall, which has been extensively reported in the literature. In most of the previous studies [16–18], the thickness of the fin is considered to be negligible or small in comparison with the fin length (the so-called thin fin), and the effect of the fin length on the natural convection flow in the cavity is considered. If the length of a fin is sufficiently large, secondary circulations arise at both the upper and lower corners of the fin [19]. It is reported that the heat transfer through the finned sidewall is reduced as the fin length increases due to the depression of the natural convection flow adjacent to the finned sidewall [19–21]. However, Ooshuizen and Paul [22] revealed that the secondary circulations resulting from the presence of a large thin fin on one wall of the cavity enhance convective flows adjacent to the opposite sidewall and thus enhance the heat transfer through the opposite sidewall.

It is noted that steady laminar natural convection flows at low Rayleigh numbers induced by a fin are the focus of the early studies

* Corresponding author. Tel.: +61 747814420; fax: +61 747816788.
E-mail address: feng.xu@jcu.edu.au (F. Xu).

0017-9310/$ - see front matter © 2008 Elsevier Ltd. All rights reserved.
doi:10.1016/j.ijheatmasstransfer.2008.06.030

Nomenclature

A	Aspect ratio, H/L
g	Acceleration due to gravity (m/s^2)
H,L	Height and length of the cavity (m)
k	Thermal conductivity (W/m/K)
Nu_{fin}	Spatially averaged Nusselt number of the hot sidewall with a fin
Nu_{nofin}	Spatially averaged Nusselt number of the hot sidewall without a fin
p	Pressure (N/m^2)
Pr	Prandtl number, ν/κ
Ra	Rayleigh number, $g\beta\Delta TH^3/\nu\kappa$
Ra_{loc}	Local Rayleigh number, $g\beta(T_{max}-T_{min})\Delta y^3/\nu\kappa$
t	Time (s)
Δt	Time-step (s)
T	Temperature (K)
T_0	Initial temperature (K)
T_c,T_h	Temperatures of the cold and hot sidewalls (K)
T_{max},T_{min}	Maximum and minimum temperatures of the fluid layer above the fin (K)
ΔT	Initial temperature difference between the working fluid and sidewall (K)
u, v	Velocity components in the x and y directions (m/s)
x, y	Horizontal and vertical coordinates (m)
Δy	Thickness of the unstable fluid layer (with an adverse temperature gradient) above the fin
β	Coefficient of thermal expansion (1/K)
ε	Enhancement factor of heat transfer
κ	Thermal diffusivity (m^2/s)
ν	Kinematic viscosity (m^2/s)
ρ	Density (kg/m^3)

[18]. Since the Rayleigh number plays an important role in the natural convection flow in the cavity [3,11,14], it is of fundamental and practical significance to examine the effect of the fin on the flow and heat transfer over an extended range of Rayleigh numbers. In particular, it is necessary to investigate the transition of the natural convection flow to steady state induced by a fin at high Rayleigh numbers. Accordingly, a shadowgraph observation of the transient natural convection flow in a suddenly differentially heated cavity with a small square fin on the heated sidewall was recently performed by Xu et al. [23], who classified the transition of the flow resulting from sudden heating into three distinct stages: an early stage, a transitional stage and a quasi-steady stage. It is found that, in the early stage, the fin blocks the upstream vertical boundary layer flow and forces it to detach from the finned sidewall, and thus a lower intrusion front is formed. The lower intrusion front almost immediately reattaches to the downstream sidewall after it bypasses the fin. A double-layer structure of the vertical boundary layer, similar to that observed without a fin [24], is ultimately formed in the transition to the quasi-steady state. The observed flow features are also consistent with those reported in [25], in which no clear separation around the small square fin in the laminar flow regime is observed.

As indicated in the previous studies [18], the fin length is an important parameter affecting the natural convection flow in the cavity, and thus a further experiment has been performed by the present authors [26] in order to investigate the effect of the fin length on the transient natural convection flow in the cavity. It is found that the transition of the natural convection flow induced by a large thin fin exhibits features distinct from that induced by a small square fin, and flow separation and oscillations of the thermal flow above the thin fin have been observed. Furthermore, oscillations in turn trigger travelling waves in the downstream boundary layer and the potential for transition to a turbulent downstream flow. However, since the experimental observations provide only qualitative information on the transient flow, it is necessary to perform a further quantitative investigation in order to obtain insights into the correlation between the fin and the flow separation and oscillations around the fin. This motivates the present numerical simulation.

In this paper, the experimental set-up reported in [26] is numerically simulated by a two-dimensional cavity. The numerical procedures are described in Section 2; numerical results are compared with the experimental data in Section 3; the oscillations of the thermal flow around the fin are examined in detail in Section 4; and the enhancement of heat transfer is calculated in Section 5. Finally, the conclusions are presented in Section 6.

2. Numerical procedures

The experiment by Xu et al. [26], whose experimental model is sketched in Fig. 1(a), is considered. The walls of the cavity are made of 19.5-mm thick acrylic sheet (Perspex^{TM}) except for the two 1-mm thick copper sidewalls adjacent to the water baths. A 2-mm thick acrylic fin of length 40 mm is attached horizontally at the mid-height of the heated sidewall, as seen in Fig. 1(a). Since the thermal conductivity of acrylic sheet is only about 0.2 Wm^{-1} K^{-1}, much less than that of copper (385 Wm^{-1} K^{-1}) [26], the heat transfer through the acrylic walls and fin is negligibly small in comparison with that through the copper sidewalls. Accordingly, the acrylic walls and fin are considered adiabatic and the two copper sidewalls are regarded as isothermal in the present numerical simulation.

Previous studies [8,11] show that two-dimensional simulations are able to characterize well the flow features of the transient natural convection in the cavity. Furthermore, since the shadowgraph procedure used in [26] presents images which are essentially transverse integrals of the flow, it is able to describe only the two-dimensional structure of the flow. Accordingly, a two-dimensional numerical simulation is performed in this paper by solving the two-dimensional governing equations with the Boussinesq approximation:

$$\frac{\partial u}{\partial x}+\frac{\partial v}{\partial y}=0, \tag{1}$$

$$\frac{\partial u}{\partial t}+u\frac{\partial u}{\partial x}+v\frac{\partial u}{\partial y}=-\frac{1}{\rho}\frac{\partial p}{\partial x}+\nu\left(\frac{\partial^2 u}{\partial x^2}+\frac{\partial^2 u}{\partial y^2}\right), \tag{2}$$

$$\frac{\partial v}{\partial t}+u\frac{\partial v}{\partial x}+v\frac{\partial v}{\partial y}=-\frac{1}{\rho}\frac{\partial p}{\partial y}+\nu\left(\frac{\partial^2 v}{\partial x^2}+\frac{\partial^2 v}{\partial y^2}\right)+g\beta(T-T_0), \tag{3}$$

$$\frac{\partial T}{\partial t}+u\frac{\partial T}{\partial x}+v\frac{\partial T}{\partial y}=\kappa\left(\frac{\partial^2 T}{\partial x^2}+\frac{\partial^2 T}{\partial y^2}\right). \tag{4}$$

In the experiment described by Xu et al. [26] the working fluid (water) is initially motionless and isothermal with a temperature T_0 = 295.55 K, which is thus adopted as the initial condition in the present numerical simulation. Once the experiment starts (at t = 0), the temperature of the sidewall with the fin is suddenly raised by ΔT by the water in the hot water bath and the tempera-

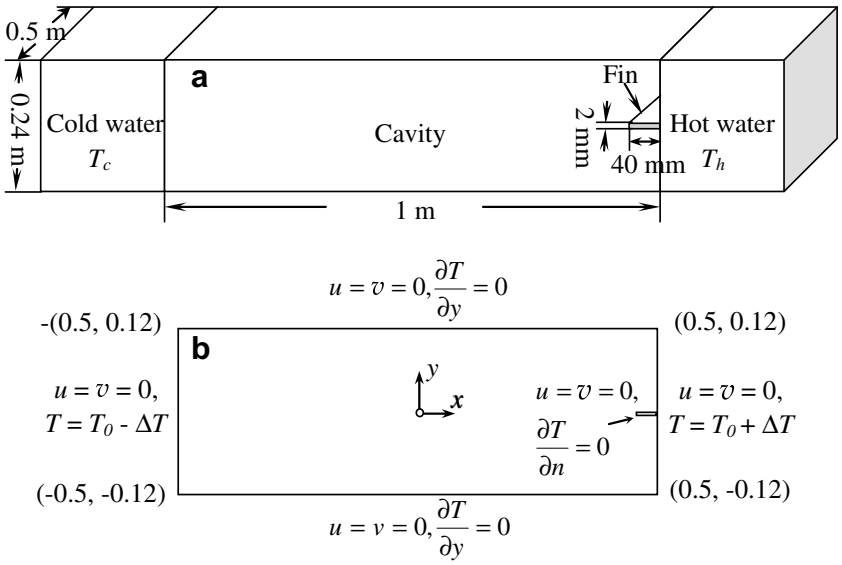

Fig. 1. (a) Schematic of the experimental model in Xu et al. [26]. (b) Computational domain and boundary conditions.

ture of the other sidewall is reduced by the same amount by the water in the cold water bath. Bachelor [1] pointed out that the subsequent development of natural convection in the cavity is determined by three governing parameters: the Rayleigh number (Ra), the Prandtl number (Pr) and the aspect ratio (A). They are defined as follows,

$$Ra = \frac{g\beta(T_h - T_c)H^3}{\nu\kappa}, \quad Pr = \frac{\nu}{\kappa}, \quad A = \frac{H}{L}. \tag{5}$$

It is worth noting that since a thermal boundary layer is formed on the water bath side of the sidewall even though the hot water bath is vigorously stirred, the temperature of the heated sidewall may be lower than the average water temperature in the hot water bath. Similarly, the temperature of the cooled sidewall may be higher than the average water temperature in the cold water bath. As a result, the actual temperature difference between the two copper sidewalls is smaller than that between the average temperatures of the two water baths. The effect is that the actual Rayleigh number achieved in the experiment [26] is smaller, by a factor of approximately 2, than that calculated if the sidewall temperatures are assumed to be equal to the average temperatures of the associated water baths, as is effectively the case for the numerical simulations. This was not commented explicitly on in [26] as there were no numerical results reported. The possibility of a reduction in the effective Rayleigh number was also raised in [7,8]. Thus in simulating a given experiment, the Rayleigh number used could be approximately half of that calculated from the difference between the water bath temperatures in the experiment.

Based on the above discussion of the experimental cavity, the top and bottom of the two-dimensional computational domain and the fin are assumed adiabatic and the two side boundaries are regarded as isothermal. All the interior boundaries of the two-dimensional computational domain including the surfaces of the fin are considered to be no-slip. The computational domain and boundary conditions are illustrated in Fig. 1(b). The coordinate origin is at the center of the cavity and SI units are adopted in this paper unless otherwise specified.

The governing equations are implicitly solved using a finite-volume SIMPLE algorithm [27]. All second derivatives and linear first derivatives are approximated by a second-order center-differencing scheme. The advection terms are discretized by a QUICK scheme [8]. The time integration is by a second-order backward differencing scheme. The discretized equations are iterated with under-relaxation factors.

A hybrid grid system with finer non-uniform grids concentrated in the proximity of all wall boundaries and relatively coarse uniform grid in the interior region is constructed. In the wall boundary regions, the grid expands at a constant rate from the wall toward the interior edges of these regions. Similarly, the vicinity of the fin is finely meshed in order to accurately capture the features of the thermal flow around the fin.

Grid dependence tests have been conducted on two grid systems (211×538 and 259×743). In order to evaluate the effect of the two grid systems on the natural convection flow in the cavity, two representative quantities are evaluated numerically: the volumetric flow rate (Q) and Nusselt number (Nu) across the vertical centerline of the cavity, which are defined as (also see [28,29])

$$Q = \frac{1}{2}\int_{-H/2}^{H/2} |u| \mathrm{d}y, \tag{6}$$

$$Nu = \frac{\frac{1}{H}\int_{-H/2}^{H/2} |\rho C_p u T - k\frac{\partial T}{\partial x}| \mathrm{d}y}{k(2\Delta T)/L}. \tag{7}$$

Fig. 2(a) compares the time series of the flow rates calculated using the two grid systems for $Ra = 1.84 \times 10^9$ and $Pr = 6.63$. Clearly, the numerical solutions obtained with both of the grid systems reveal the same features of the flow development, including an early spike induced by the horizontal intrusion flow, with small variations in the presence of flow oscillations. Similar observations can be made from the Nusselt number time series shown in Fig. 2(b). It is also clear that for $t > 5000$ s, the curves of the calculated quantities using the two different grid systems overlap each other. These suggest that either of the two grid systems may be used in the present numerical simulation since the goal behind the present numerical simulations is to obtain insights into the flow regime dominated by the fin. In consideration of the computing time, the grid system of 211 (H) × 536 (L) with a grid inflation factor of 1.04 in the wall boundary regions is adopted.

Time-step-dependence tests have also been conducted with time-steps of 0.1 s and 0.05 s, respectively (which are smaller than the time-step of 0.7 s adopted in [8] for a comparable Rayleigh number). The test results are also shown in Fig. 2. As seen in Fig. 2(a) and (b), although the variations of the calculated

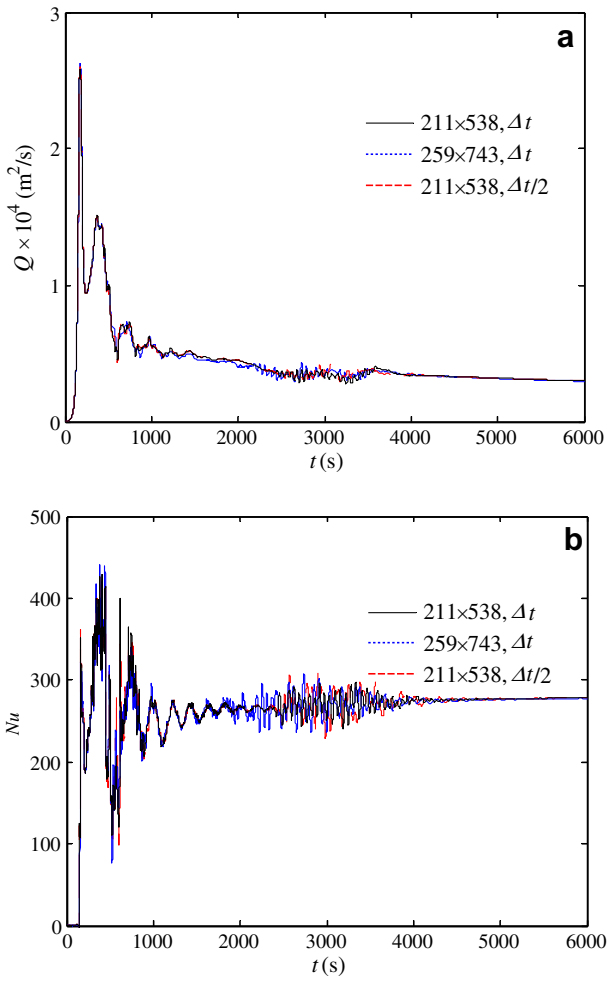

Fig. 2. Grid and time-step dependence tests for $Ra = 1.84 \times 10^9$ and $Pr = 6.63$ (where $\Delta t = 0.1$ s). Plotted are time series of (a) the volumetric flow rate and (b) the Nusselt number over the vertical centerline.

quantities between the two sets of numerical results with different time-steps are discernible in the presence of flow oscillations, they are considerably small (<1%). Therefore, the time-step of 0.1 s is considered to be sufficiently small to capture the major flow features, and is adopted in the present study.

3. Numerical results and comparisons with the experiments

3.1. Comparisons between the calculated and experimentally visualized flow structures

An important feature of the early transient thermal flow in the cavity is the formation and evolution of intrusion fronts under the fin and under the ceiling. Fig. 3 presents the numerically calculated isotherms for $Ra = 1.84 \times 10^9$ calculated in terms of the temperature difference between the two sidewalls ($T_h - T_c = 8$ K) and the corresponding shadowgraph images for $Ra = 3.67 \times 10^9$ calculated in terms of the temperature difference (16 K) between the two water baths [26]. Clearly, there is good agreement between the experiment and simulation, supporting the discussion in Section 2 regarding the Rayleigh number values actually achieved in the experiment. For the purpose of comparing the calculated flow with the experimentally visualized flow at the same time, the numerical results at $Ra = 1.84 \times 10^9$ are presented in the following figures.

Fig. 3(a) and (b) show that two intrusion fronts are formed: one underneath the ceiling and the other underneath the thin fin. The upper and lower sections of the boundary layer are almost identical. After the lower intrusion front bypasses the thin fin, this similarity disappears and a starting plume is formed, as shown in Fig. 3(c) and (d). The numerical and experimental flows agree well in terms of the plume behavior at this time. Fig. 3(e) and (f) show that, in the subsequent flow development, the front of the starting plume ascends until it strikes the intrusion under the ceiling. Distinct variations of the plume structures between the numerical and experimental results are clear when the plume front is approaching the intrusion under the ceiling. The experimental plume head destabilizes and breaks up, but the numerical predicted plume remains stable. This discrepancy could be attributed to the presence of stronger perturbations in the experiment. However, a full investigation of this destabilization is beyond the scope of this paper.

The time dependence of the positions of the calculated and experimentally visualized intrusion and starting plume fronts is plotted in Fig. 4. Here, the position of the calculated front corre-

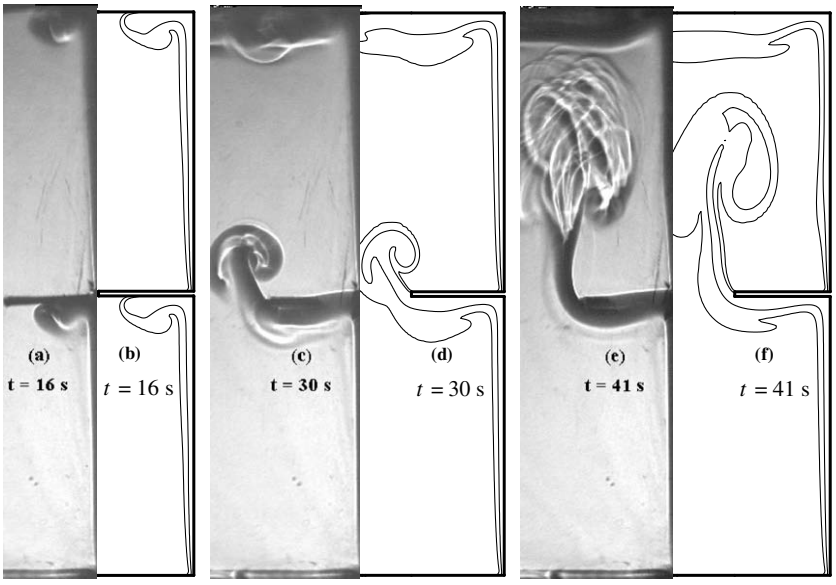

Fig. 3. Early development of the thermal flow around the fin. (a), (c) and (e) Shadowgraphs. (b), (d) and (f) Isotherms (contours of 295.56 and 296 K).

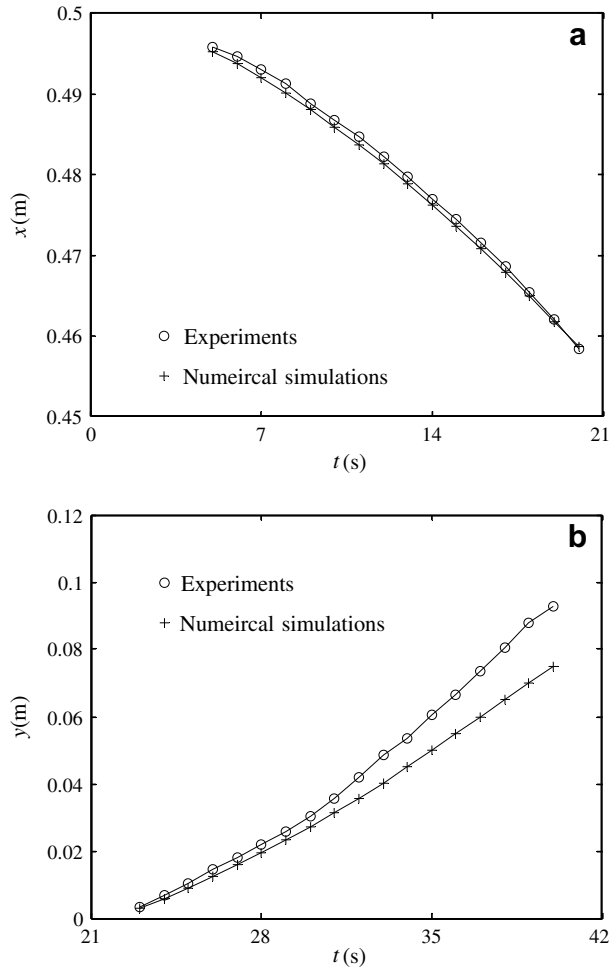

Fig. 4. Dependence of the positions of the thermal flow fronts on time. (a) Lower intrusion front. (b) Starting plume front.

sponds to the front end of the isotherm of 295.56 K (see Fig. 3b, d and f), and the position of the experimentally visualized front is determined by the bright strip in front of the thermal flow head (see Fig. 3a, c and e). Clearly, before the front bypasses the fin to form an ascending plume, the position of the calculated intrusion front agrees very well with that of the experimentally visualized intrusion front (Fig. 4a). Xu et al. [26] showed that the motion of the experimental lower intrusion front is characterized by the velocity scale of $Pr^{1/3}\ Ra^{2/3}(t\kappa/H^2)^{3/2}$. Due to the good agreement between the experimental and calculated lower intrusion fronts, the velocity scale given by Xu et al. [26] is also consistent with the present calculated results. Indeed, this good agreement between the experiment and simulation remains for the early stage of the starting plume ($t < 30$ s in Fig. 4b). However, as the plume head destabilises in the experiment, the plume front ascends more quickly than that predicted by the numerical simulation. This is evidenced by the deviation of the two plots for $t > 30$ s in Fig. 4(b).

After the plume front strikes the intrusion under the ceiling, it is entrained into the intrusion and convected away. Although the reattachment of the plume front to the vertical boundary layer does not occur, the thermal flow behind the plume front is ultimately drawn to the downstream boundary layer due to entrainment by the vertical boundary layer. With the passage of time, the cold intrusion from the opposite sidewall strikes the finned sidewall. Fig. 5(a) and (b) present the flow structures when the cold intrusion front (marked by the dark solid line near the lower corner in the shadowgraph image) is approaching the hot sidewall. Note that the shadowgraph image here has been processed by subtracting an image recorded immediately before the experiment starts from the actual shadowgraph image (see [24] for details). Clearly, the development of the calculated flow is slightly quicker than that of the experimental one although the basic flow structures are similar between the two sets of results. Both the experimental and numerical results indicate that the thermal flow around the fin has been drawn closer to the fin at this time.

A double-layer structure of the boundary layer starts to form in the subsequent development of the flow after the cold intrusion strikes the finned sidewall (also see [10,24]). Fig. 5(c) shows that a bright outer strip arises outside the thermal boundary layer in the lower cavity. Corresponding to the bright outer strip, an upward thermal tongue of isotherms is present near the bottom corner (refer to Fig. 5d). As described in [10], the outer bright strip in the shadowgraph images corresponds to the positions of the

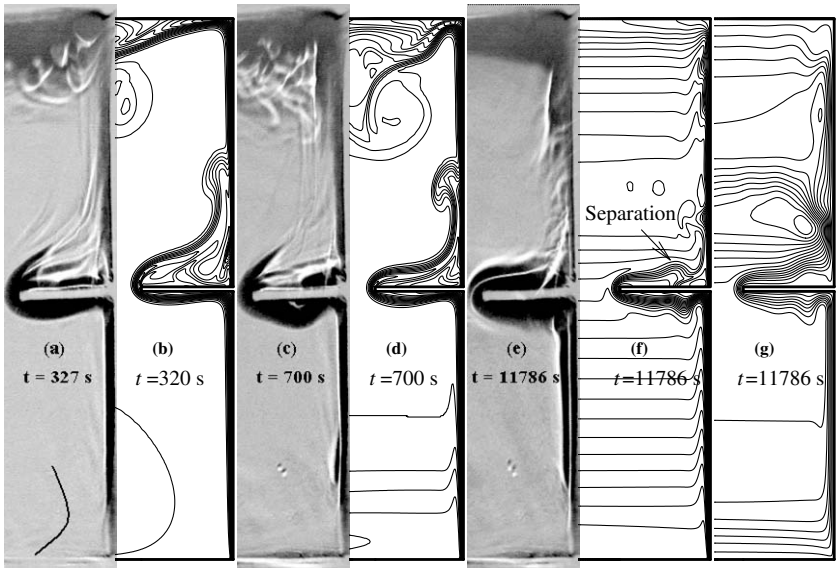

Fig. 5. Transition of the thermal flow around the fin to a periodic flow. (a), (c) and (e) Shadowgraph. (b), (d) and (f) Isotherms (contours from 291.73 to 299.53 K with an interval of 0.2 K). (g) Streamlines (contours from 2.4×10^{-6} to 3.6×10^{-5} m^2/s with an interval of 2.4×10^{-6} m^2/s).

minima of the second derivative of the temperature. Furthermore, it is seen in Fig. 5(d) that, due to the strong perturbations from the entrainment of the thermal flow to the sidewall, the flow structure near the top corner still displays turbulent features.

As time increases further, the stratification of the interior fluid increases, and the lower outer bright strip ultimately reaches the fin. The double-layer structure in the lower cavity becomes more distinct, as seen in Fig. 5(e). Fig. 5(f) shows that an upward thermal tongue of isotherms also arises near the top corner, which corresponds to a bright strip in Fig. 5(e). However, the bright strip in the upper cavity remains broken for a long time (more than 3 h in the experiment in [26]). The streamlines in Fig. 5(g) indicate that a circulation above and close to the fin is responsible for the break-up of the bright strip observed in the shadowgraph image. Furthermore, the separation of the thermal flow above the fin is clear, as seen in Fig. 5(e) and (f).

3.2. Comparisons between the calculated and measured temperatures

For the purpose of illustrating the overall transition of the boundary layer adjacent to the finned sidewall to a time-dependent periodic flow, Fig. 6(a) presents a time series of the calculated temperature at the point (0.498 m, 0.09 m) in the boundary layer downstream of the fin, which is compared with the temperature series in Fig. 6(b) obtained at the same location without a fin. A logarithmic time scale is adopted in Fig. 6 in order to clearly show the early flow behaviors. The early transient flows with the presence of the fin include the LEE (marked by an overshoot and subsequent travelling waves, also see [7]), perturbations from the ascending plume, and reattachment of the thermal flow behind the plume front. It has been shown in Fig. 3 that the plume front is not entrained into the downstream vertical boundary layer after it bypasses the thin fin, and thus a complete LEE is observed at the downstream side of the fin at the early stage. As the plume front ascends and the thermal flow behind the plume front is attached to the downstream boundary layer, these flow behaviors may trigger large perturbations in the downstream boundary layer. Subsequently, through a slow transitional stage, the boundary layer flow approaches a time-dependent periodic flow, as seen in Fig. 6(a). It is clear that, compared with the transition to a steady state in the case without a fin in Fig. 6(b) (also see e.g. [8,30]), the fin changes the flow regimes adjacent to the sidewall and results in the transition to a time-dependent periodic flow. The mechanisms, responsible for the transition, will be discussed in Section 4.

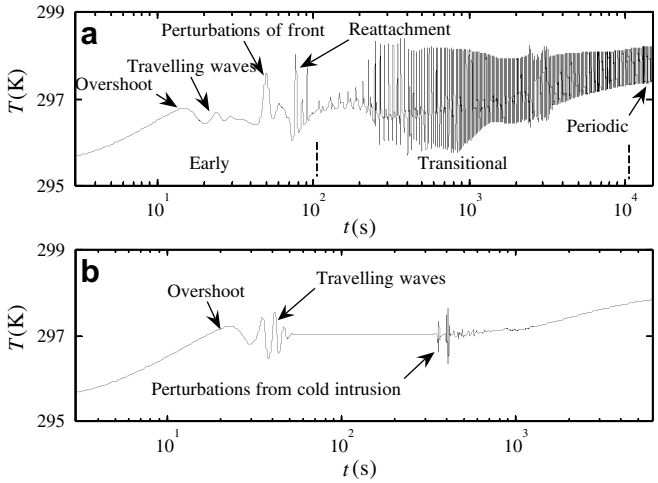

Fig. 6. Time series of the temperature at the point (0.498 m, 0.09 m). (a) For the case with a thin fin. (b) For the case without a fin.

Fig. 7(a) and (b) present the calculated and measured temperatures [26] at different positions in the boundary layer downstream of the fin during the early stage of the flow development. Qualitative agreement between the calculated and measured temperature time series in terms of the major flow features including the LEE effect, traveling waves and perturbations of the plume front is clear. However, the discrepancies between the experimental and numerical results are also discernible, particularly in the very early stage of the flow development. This is because an ideally isothermal and motionless condition at the initial state cannot be achieved in the experiment.

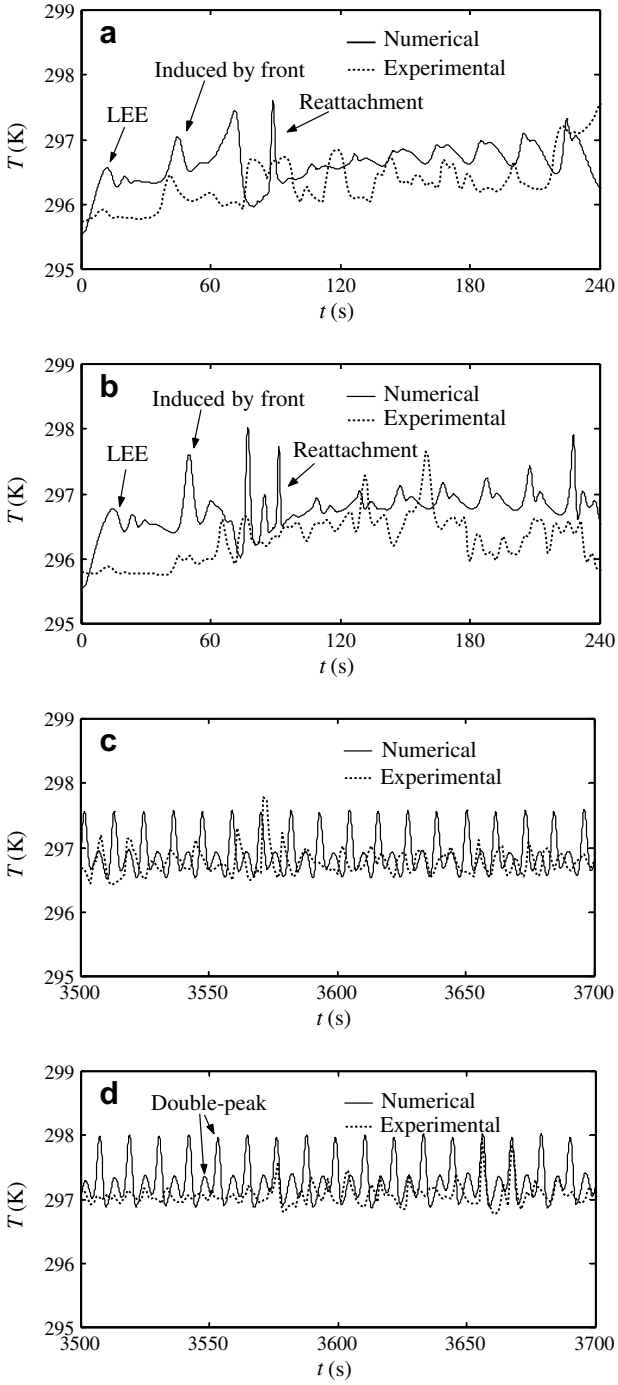

Fig. 7. Time series of the calculated and measured temperatures at different positions in the different stages. (a) and (c) At (0.498 m, 0.06 m). (b) and (d) At (0.498 m, 0.09 m).

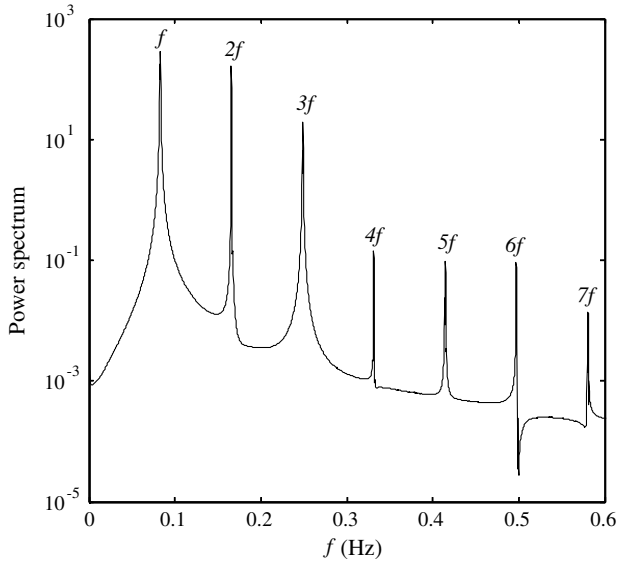

Fig. 8. Power spectrum of the calculated temperature time series at the location (0.498 m, 0.09 m) in the transition to a periodic flow.

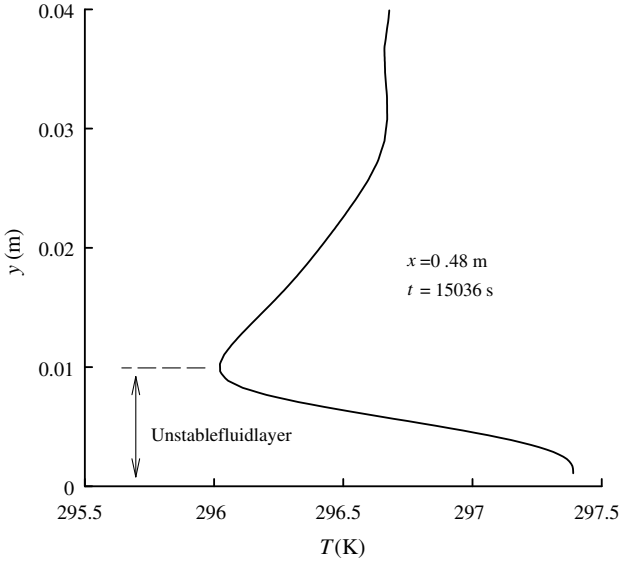

Fig. 9. Temperature profile above the fin in the transition to a periodic flow (the fin is at the mid-height, $y = 0$).

In order to further compare the calculated temperature with the measured temperature during the transition to a periodic flow, Fig. 7(c) and (d) plot the time series of the calculated and measured temperatures at two different points in the downstream boundary layer over a period of 200 s from $t = 3500$ to 3700 s. The calculated temperatures show features consistent with the experimental measurements. However, the amplitude of the oscillations of the calculated temperature is apparently larger (up to 32%) than that of the oscillations of the measured temperature. This could be attributed to the errors associated with the positioning of the thermositors; the temperature gradient near the sidewall is very high and small variations in the location of a thermistor can result in very large differences in the measured temperature [7].

Fig. 8 presents the power spectrum of the calculated temperature in the transition to a periodic flow. The dominant frequency is found to be $f = 0.0832$ Hz, consistent with that of the experimental measurement (0.095 Hz, see [26]). It is clear in Fig. 8 that harmonic frequency modes such as $2f$, $3f$ and higher are present. The frequency mode of $2f$ is in fact clearly visible in Fig. 7(d), indicated by the double peaks (one higher and the other one lower) of the temperature signals.

4. Oscillations of the thermal flow around the fin

As shown in Fig. 5(e) and (f), travelling waves in the boundary layer downstream of the fin are triggered by the oscillations of the thermal flow around the fin. For the purpose of examining the mechanism responsible for the oscillations, Fig. 9 presents the temperature profile of the fluid layer above the fin at $x = 0.48$ m. Clearly, for $y < 0.01$ m, the temperature increases toward the fin surface. This temperature configuration is potentially unstable, and the stability of the fluid layer is governed by a local Rayleigh number ($Ra_{loc} = g\beta(T_{max} - T_{min})\Delta y^3/\nu\kappa$). In the present case, the local Rayleigh number is estimated to be 2.2×10^4, which is much larger than the critical value of $O(10^3)$ for Rayleigh–Benard instabilities [31]. Accordingly, the thermal flow above the fin is unstable in a Rayleigh–Benard sense, with the instabilities appearing as the plume-like intermittent separations seen in Fig. 5(e), (f) and (g). These separations are then entrained by the downstream boundary layer.

In order to illustrate the oscillations of the flow adjacent to the finned sidewall, Fig. 10 shows the spatial distribution of the calculated standard deviation of the temperatures. Clearly, the oscillations of the temperatures are the strongest at the downstream side of the fin, and intermittent plumes induce the oscillations along the wall downstream of the fin. This is consistent with the time series of the temperatures at different positions downstream of the fin shown in Figs. 6 and 7.

Previous numerical simulations have showed that a bifurcation (oscillatory flow) of the natural convection flow in a square cavity filled with air ($Pr \approx 0.7$) may be observed if the Rayleigh number is $O(10^8)$ or higher (see e.g. [11]). The oscillatory flow in a cavity without a fin has been demonstrated to be sensitive to the Prandtl number and aspect ratio [12,32]. For example, the flow in a square

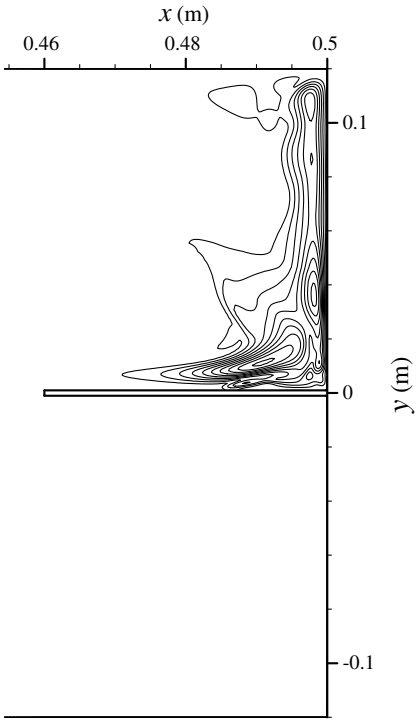

Fig. 10. Standard deviation of the temperatures from 14900 to 15000 s (contours from 0.05 to 0.5 K with an interval of 0.05 K).

cavity filled with water ($Pr \approx 7$) remains steady even though the Rayleigh number is much higher than O(10^8) (see e.g. [30]). As seen in Fig. 6(b), at the Rayleigh number of 1.84×10^9, the natural convection flow in the water filled shallow cavity without a fin remains steady. In contrast to that in Fig. 6(b), for the case with a fin, strong intermittent plumes are generated at the leeward of the fin, which in turn trigger the oscillations in the downstream vertical boundary layer (Fig. 10). The amplitude of the temperature fluctuation at the point (0.498 m, 0.09 m) is up to 11% of the temperature difference between the two sidewalls (refer to Fig. 6a). As a consequence, the natural convection flow in the cavity with a thin fin ultimately approaches an oscillatory flow.

5. Enhancement of heat transfer

For the purpose of examining the impact of the oscillations on heat transfer through the sidewall, Fig. 11 presents a comparison of the calculated local Nusselt numbers along the hot sidewall with and without a thin fin at two different times (corresponding to the early and quasi-steady stages of the flow development, respectively). The profiles of the Nusselt number upstream of the fin are almost identical for the cases with and without the fin as expected. This implies that the fin has a negligible effect on the heat transfer through the upstream section of the sidewall. However, the profiles of the local Nusselt number near and downstream of the fin are apparently different from those in the case without a fin. The net effect is that the average Nusselt number downstream of the fin is larger than that in the case without a fin. This is particularly true in the early time (Fig. 11a), suggesting that the oscillations of the downstream thermal flow enhance heat transfer through the downstream sidewall.

In order to quantitatively assess the enhancement or depression of the heat transfer through the finned sidewall, the Nusselt number along the sidewall is integrated and an enhancement factor is defined as follows,

$$\varepsilon = (Nu_{\text{fin}} - Nu_{\text{nofin}})/Nu_{\text{nofin}}. \quad (8)$$

It is clear from the definition that the enhancement factor (ε) denotes the percentage of enhancement (if positive) or depression (if negative) of the heat transfer through the finned sidewall with reference to the case without the fin.

Fig. 12(a) plots the time series of the enhancement factor calculated with a single thin fin on the hot sidewall and no fin on the cold sidewall. ε is positive almost all the time with a maximum value of 23% in the early stage. This suggests that the heat transfer through the finned sidewall is significantly enhanced in the early stage, which is supported by the observation in Fig. 11(a). It is also worth noting that, despite fluctuations, ε steadily reduces from 23% in the early time to 4.6% at 6000 s. This is because more heat input through the finned hot sidewall compared to the heat output through the unfinned cold sidewall causes the average temperature of the fluid in the cavity to increase, resulting in a smaller temperature difference between the finned sidewall and the fluid. The reduced temperature difference in turn reduces the heat input through the finned sidewall.

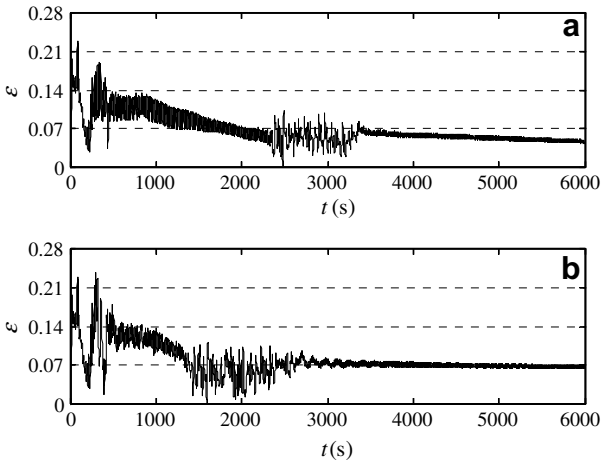

Fig. 12. Time series of the enhancement factor. (a) With one fin on the heated wall and no fin on the cooled wall. (b) With one fin on the heated wall and the other symmetrically on the cooled wall.

In order to eliminate the effect of the increase of the average fluid temperature, a further investigation for which an identical adiabatic fin is attached horizontally at the mid-height of the cold sidewall has been performed. In this case, the heat input through the hot sidewall balances the heat output through the cold sidewall, and the average fluid temperature remains constant. Fig. 12(b) shows the calculated ε as a function of time. It is seen from this figure that ε approaches a steady positive value of approximately 7%, suggesting that an adiabatic thin fin, through improving downstream convection flows, is able to enhance heat transfer through the cavity by approximately 7% for the present Rayleigh number.

Fig. 13 presents the time series of the calculated flow rate cross the centerline in the cases with and without a thin fin. It is seen

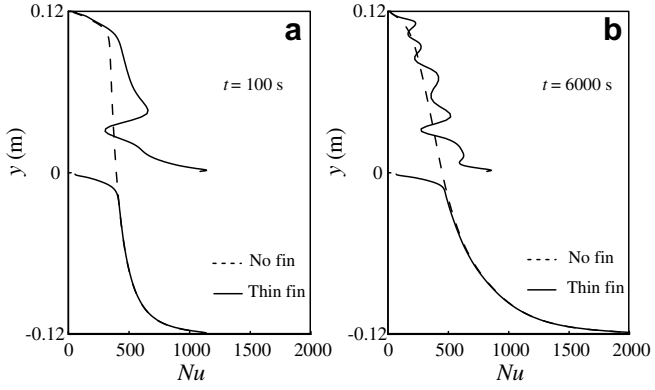

Fig. 11. Profiles of the Nusselt number along the hot sidewall with and without a thin fin at different times.

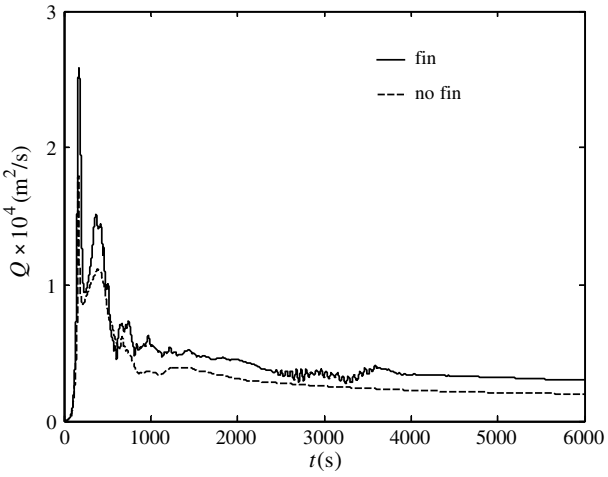

Fig. 13. Time series of the flow rate cross the center line ($x = 0$) in the cases with and without a fin.

from this figure that, consistent with the enhancement of the heat transfer through the finned sidewall, the horizontal convection flow across the cavity is significantly improved due to the presence of the fin, with an increase of approximately 41% at $t = 6000$ s.

6. Conclusions

In this paper, the natural convection flow in a suddenly differentially heated cavity with a thin fin on the hot sidewall is numerically investigated. The present numerical results are shown to be consistent with the previous flow visualizations and temperature measurements. The numerical results also demonstrate that the thin fin is able to change the flow regime in the cavity and cause the transition to a periodic flow.

In the early stage of the flow development following sudden heating, a lower intrusion front is formed under the fin, and a starting plume arises after the lower intrusion front bypasses the fin. The starting plume induces strong perturbations and even turbulence in the downstream vertical boundary layer. Accordingly, heat transfer through the finned sidewall is significantly enhanced in the early stage (a maximum increase of up to 23% in the present study).

In the transition to a periodic flow, separation and intermittent plumes of the thermal flow above the fin are observed. The intermittent plumes are due to the Rayleigh–Benard-type instability, and the natural convection flow in the cavity approaches a time-dependent periodic flow. Furthermore, the intermittent plumes also trigger oscillations in the downstream boundary layer, which thus enhance heat transfer through the finned sidewall (a 7% increase of heat transfer rate at the quasi-steady state for the present Rayleigh number). The horizontal convection flow cross the cavity is also significantly reinforced, and the flow rate cross the centerline increases by up to 41% at the quasi-steady stage.

The present investigation indicates that placing an adiabatic thin fin horizontally on a heat transfer surface provides a simple and practical way for enhancing heat transfer. Since the focus of the present paper is on some fundamental aspects of the flow configuration around the fin, no attempt is made to resolve the optimal configuration of fins for the purpose of enhancing heat transfer.

Acknowledgement

The authors are grateful to the Australian Research Council for its financial support.

References

[1] G.K. Bachelor, Heat transfer by free convection across a closed cavity between vertical boundaries at different temperatures, Q. Appl. Math. 12 (1954) 209–233.
[2] A.E. Gill, The boundary-layer regime for convection in a rectangular cavity, J. Fluid Mech. 26 (1966) 515–536.
[3] G. De Vahl Davis, Natural convection of air in a square cavity: a bench mark numerical solution, Int. J. Numer. Meth. Fluids 3 (1983) 249–264.
[4] J.C. Patterson, J. Imberger, Unsteady natural convection in a rectangular cavity, J. Fluid Mech. 100 (1980) 65–86.
[5] S.W. Armfield, J.C. Patterson, Wave properties of natural convection boundary layers, J. Fluid Mech. 239 (1992) 195–212.
[6] W. Schöpf, J.C. Patterson, Natural convection in a side-heated cavity: visualization of the initial flow features, J. Fluid Mech. 295 (1995) 279–357.
[7] J.C. Patterson, T. Graham, W. Schöpf, S.W. Armfield, Boundary layer development on a semi-infinite suddenly heated vertical plate, J. Fluid Mech. 219 (2002) 467–497.
[8] J.C. Patterson, S.W. Armfield, Transient features of natural convection in a cavity, J. Fluid Mech. 219 (1990) 469–497.
[9] W. Schöpf, J.C. Patterson, Visualization of natural convection in a side-heated cavity: transition to the final steady state, Int. J. Heat Mass Transfer 39 (1996) 3497–3509.
[10] F. Xu, J.C. Patterson, C. Lei, On the double-layer structure of the thermal boundary layer in a differentially heated cavity, Int. J. Heat Mass Transfer 51 (2008) 3803–3815.
[11] S. Paolucci, D.R. Chenoweth, Transition to chaos in a differentially heated vertical cavity, J. Fluid Mech. 201 (1989) 379–410.
[12] P. Le Quere, Transition to unsteady natural convection in a tall water-filled cavity, Phys. Fluids 2 (1990) 503–515.
[13] P. Le Quere, M. Behnia, From onset of unsteadiness to chaos in a differentially heated square cavity, J. Fluid Mech. 359 (1998) 81–107.
[14] S. Paolucci, Direct numerical simulation of two-dimensional turbulent natural convection in an enclosed cavity, J. Fluid Mech. 215 (1990) 229–262.
[15] H.S. Dol, K. Hanjalic, Computational study of turbulent natural convection in a side-heated near-cubic enclosure at a high Rayleigh number, Int. J. Heat Mass Transfer 44 (2001) 2323–2344.
[16] X. Shi, J.M. Khodadadi, Laminar natural convection heat transfer in a differentially heated square cavity due to a thin fin on the hot wall, J. Heat Transfer 125 (2003) 624–634.
[17] S.H. Tasnim, M.R. Collins, Numerical analysis of heat transfer in a square cavity with a baffle on the hot wall, Int. Commun. Heat Mass Transfer 31 (2004) 639–650.
[18] E. Bilgen, Natural convection in cavities with a thin fin on the hot wall, Int. J. Heat Mass Transfer 48 (2005) 3493–3505.
[19] A. Nag, A. Sarkar, V.M.K. Sastri, Natural convection in a differentially heated square cavity with a horizontal partition plate on the hot wall, Comput. Methods Appl. Mech. Engrg. 110 (1993) 143–156 .
[20] A. Bejan, Natural convection heat transfer in a porous layer with internal flow obstructions, Int. J. Heat Mass Transfer 26 (1983) 815–822.
[21] R.L. Frederick, Natural convection in an inclined square enclosure with a partition attached to its cold wall, Int. J. Heat Mass Transfer 32 (1989) 87–94.
[22] P.L. Ooshuizen, J.T. Paul, Free convection heat transfer in a cavity fitted with a horizontal plate on the cold wall, Adv. Enhanced Heat Transfer 43 (1985) 101–107.
[23] F. Xu, J.C. Patterson, C. Lei, Experimental observations of the thermal flow around a square obstruction on a vertical wall in a differentially heated cavity, Exp. Fluids 40 (2006) 363–371.
[24] F. Xu, J.C. Patterson, C. Lei, Shadowgraph observations of the transition of the thermal boundary layer in a side-heated cavity, Exp. Fluids 38 (2005) 770–779.
[25] S. Shakerin, M. Bohn, R.I. Loehrke, Natural convection in an enclosure with discrete roughness elements on a vertical heated wall, Int. J. Heat Mass Transfer 31 (1988) 1423–1430.
[26] F. Xu, J.C. Patterson, C. Lei, An experimental study of the unsteady thermal flow around a thin fin on a sidewall of a differentially heated cavity, Int. J. Heat Fluid Flow 29 (2008) 1139–1153.
[27] S.V. Patankar, Numerical Heat Transfer and Fluid Flow, Hemisphere, New York, 1980.
[28] S.G. Schladow, Oscillatory motion in a side-heated cavity, J. Fluid Mech. 213 (1990) 589–610.
[29] C. Lei, J.C. Patterson, Unsteady natural convection in a triangular enclosure induced by absorption of radiation, J. Fluid Mech. 460 (2002) 181–209.
[30] A. Javam, S.W. Armfield, Stability and transition of stratified natural convection flow in open cavities, J. Fluid Mech. 445 (2001) 285–303.
[31] P.G. Drazin, W.H. Reid, Hydrodynamic Stability, Cambridge University Press, 1981.
[32] R.J.A. Janssen, R.A.W.M. Henkes, Influence of Prandtl number on instability mechanisms and transition in a differentially heated square cavity, J. Fluid Mech. 290 (1995) 319–344.